Journal of Engineering Science and Technology
Vol. 20, No. 2 (2025) 590 - 611

DEVELOPMENT OF THE INTERNAL COMBUSTION ENGINE OIL PAN IN DEEP DRAWING PROCESS: FE SIMULATION AND EXPERIMENTAL VALIDATION

YONGYUDTH THANAUNYAPORN, JARUPONG CHAROENSUK, PHIRAPHONG LARPPRASOETKUN, SURASAK SURANUNTCHAI*

King Mongkut's University of Technology Thonburi, 126 Pracha Uthit Rd, Bang Mod, Thung Khru, Bangkok, 10140, Thailand
*Corresponding Author: surasak.sur@kmutt.ac.th

Abstract

In this study, the forming process of JAC270F sheet metal with a thickness of 1.2 mm was investigated to produce a complete "INTERNAL COMBUSTION ENGINE OIL PAN." A novel two-step forming method, termed the "Two-Steps Deep Drawing Process," was proposed, along with the application of "Finite Element Analysis (FEA)" using the AutoForm software to achieve highly realistic forming simulations. Material models, including the Barlat yield function, Swift hardening law, and forming limit diagrams from the Keeler equation, were employed. Additionally, key parameters influencing the successful formation of the Internal Combustion Engine Oil Pan without defects were examined. The use of a blank holder force of 7.5 tons, a die radius of 9.6 mm, and a reduction in the coefficient of friction to 0.11 effectively eliminated cracks and wrinkles in the part. The simulation accuracy for part thinning and springback showed deviations of 5.45% and 2.01%, respectively, when compared to the experimental results. In conclusion, the finite element method enables accurate simulation and resolution of issues encountered in actual workpieces, reducing time and material waste from the trial-and-error process in the physical production setup precisely.

Keywords: Deep drawing processes, Defects, Finite element method, Internal combustion engine oil pan, JAC270F.

1. Introduction

Automotive part manufacturers have established specific characteristics for forming cylindrical automotive components like engine oil pans, automatic transmission oil pans, and engine oil filters. The deep drawing process, depicted in Fig. 1, is commonly employed for this purpose. It involves using a die, punch, and blank holder to shape the workpiece. The process carefully controls the blank holder force, while forming a deep cavity shape by pressing a punch into a die, to ensure that the original thickness of the workpiece is maintained [1, 2].

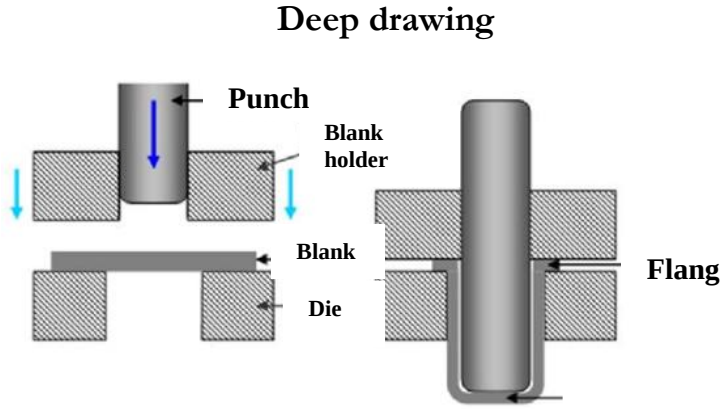

Fig. 1. Deep drawing process [3].

Deep drawing is a specialized sheet metal forming technique involving a die tool and press machine to shape metal into complex forms. Unlike regular stamping, it is predominantly a cold stamping process used for parts with intricate shapes that cannot be easily achieved otherwise. This process imparts depth to the workpiece, which undergoes permanent deformation. It requires significant external force or stress, surpassing the material's yield strength. Steel is commonly employed due to its ductility, enabling deep drawing without the risk of cracking or breaking [4].

Currently, parts are typically designed for single-action with blank holder die manufacturing processes. This operation begins with the clamping of the workpiece by the blank holder and die. As the workpiece advances towards the punch, a reaction force is generated from the bottom through the cushion post of the machine, exerting pressure back through the blank holder. Consequently, there exists a disparity in the drawing force between the punch pressure and the blank holder pressure, governing the metal flow on the workpiece [5-7]. The primary challenges encountered in the deep drawing process include cracking and wrinkling at the bottom corners and walls of the workpiece [8-9].

Multi-step press processes are a forming technique used to improve the formability of sheet metal. This technique prevents cracks by dividing the forming operation into multiple stages. Optimizing the shape of the workpiece at each stage is crucial for successful multi-step deep drawing. This paper reviews existing methods for shape design in each step of the multi-step drawing process. Preforming resulted in an improvement in the forming limit height compared to single forming [10].

The simulation will commence at the inception of the deep drawing process development for this part. The resulting simulations will determine if deep drawing can be successfully formed before advancing to the actual die manufacturing process. This approach minimizes manufacturing costs, reduces lead time for die manufacturing, and yields cost savings for automotive components [11], thereby fostering a competitive edge in the global market. Utilizing finite element forming simulation serves as a valuable tool to derive insights into the development of the engine oil pan in this context [12].

Additionally, Yoshihara et al. [13] conducted experiments to explore the influence of blank holder force (BHF) on stress-induced crack formation in the workpiece. Booranacheep et al. [14] compared wrinkling behavior between actual forming and finite element method simulations. Suranuntchai [11] utilized the finite element method to enhance the manufacturing process of brake drum parts in the deep drawing process using SPCC grade sheet metal with a thickness of 1.40 mm. Subsequently, Jurendić and Gaiani [15] employed the Barlat 1989 material model to predict deep drawing behavior at the end of a motorcycle exhaust pipe. Moreover, Suwanchinda and Suranuntchai [16] investigated the automotive part BRACKET FR BUMPER SIDE LH/RH using an FE program to forecast its behavior during the deep drawing process. Panich et al. [17] also applied the FLSD criterion to predict the material formability of mild steel sheet (SPCE270) used for an automotive fuel tank cover.

The objective of this research is to utilize the finite element method (FEM) in tandem with Forming Limit Diagram (FLD) based on Keeler equation and Barlat yield function to facilitate the design of the deep drawing process, optimize die design, and ascertain the optimal parameters for forming the Internal Combustion Engine Oil Pan.

2. Material and Experimental Procedure

The research aims to develop a deep drawing process for a low-strength cold-rolled steel sheet, grade JAC270F, with a thickness of 1.20 mm, considering its assumed anisotropic properties. Focusing on both the part and the deep drawing process, Fig. 2 illustrates the shape of the Internal Combustion Engine Oil Pan. The stamping process comprises 4 dies and 7 manufacturing processes, as depicted in Fig. 3. This study specifically investigates the deep drawing process, which is the initial phase. Tensile tests were conducted in accordance with the JIS Z 2241-2022 standard, with the test specimen depicted in Fig. 4. Material parameters necessary for prediction, following the Barlat 3-parameter equation, are provided in Table 1 and Fig. 5.

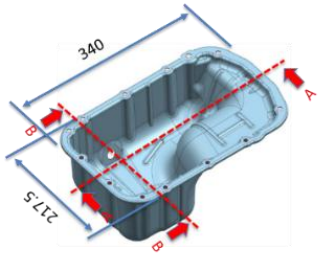

(a) Oil pan of ICE-engine.

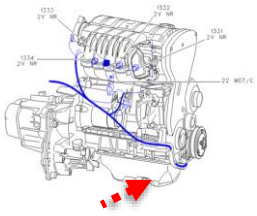

Oil Pan of ICE-Engine

(b) Dimension of Oil pan.

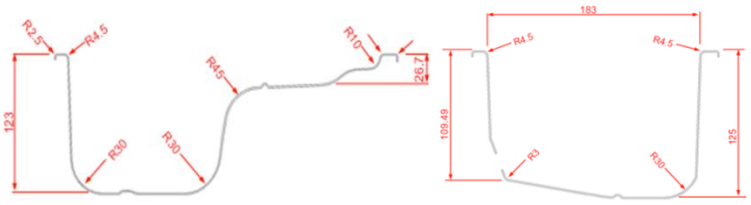

(c) Section A-A. **(d) Dimension of Oil pan.**

Fig. 2. Internal combustion engine oil pan.

From the Fig. 2, the oil pan has a specification: for engine 1200 cc, JAC270F 45/45 (Mild Steel), sheet thickness 1.20 mm, capacity content 5 L and weight 1.37 kg.

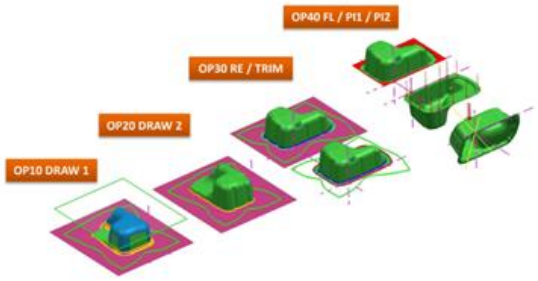

Fig. 3. Stamping processes of the part.

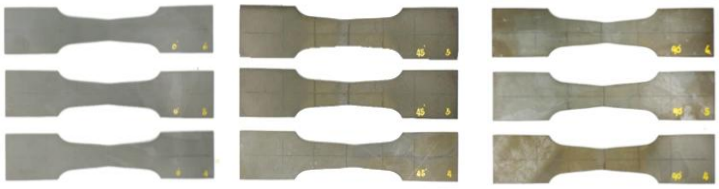

Fig. 4. Tensile test specimens in rolling direction of 0, 45 and 90 degrees, respectively.

Table 1. Mechanical properties of the test specimens under tension.

	Direction (Degree)		
Mechanical Properties	**0**	**45**	**90**
Young's Modulus (GPa)	186.20	195.80	202.40
Tensile Strength (MPa)	310.26	323.17	307.43
Yield Strength (MPa)	173.73	175.84	172.68
r-values	2.26	1.46	2.59
K	551.57	580.06	549.71
n	0.233	0.236	0.237

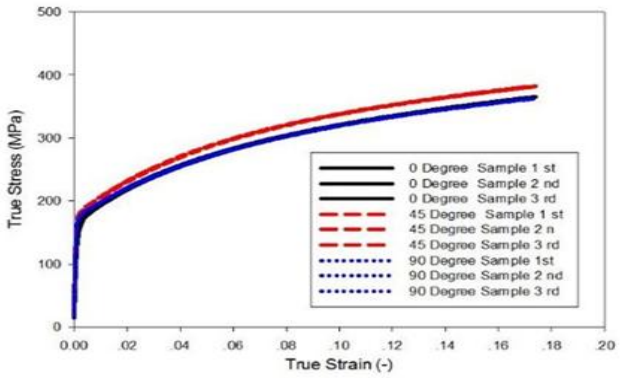

Fig. 5. True stress-true strain curves of the test specimens under tension.

2.1. Anisotropy in materials

Anisotropy manifests [18] as a mechanical phenomenon in materials, wherein their properties alter based on the direction of the applied force, thereby influencing their formability and strength. The cold rolling process, employed in sheet metal production, serves as a primary contributor to anisotropy. By transforming the originally symmetrical crystal structure into an asymmetrical one, cold rolling engenders mechanical properties that vary with the direction of force application. The plastic strain ratio (r-value) serves as a metric for quantifying this anisotropic behavior. It is computed as the ratio of width strain to thickness strain in a tensile test specimen, as illustrated by the Eq. (1):

$$r = \varepsilon_w/\varepsilon_t \quad (1)$$

where ε_w is the width strain and ε_t is the thickness strain.

Various r-values are obtained based on the rolling direction, including 0, 45, and 90 degrees. Sheet metal exhibiting high formability typically possesses a high r-value. The average r-value can be computed using the following Eq. (2):

$$\bar{r} = (r_0 + 2r_{45} + r_{90})/4 \quad (2)$$

where $\bar{r}$ is the average r-value. r_0,r_{45}, and r_{90} are the r-values in the 0-, 45-, and 90-degree directions, respectively.

Understanding anisotropy and the r-value allows engineers to predict the behavior of sheet metal during forming operations more accurately. This knowledge helps prevent defects and ensures the quality of the final product.

2.2. Strain hardening exponent

During the forming process, the material experiences a change in shape at low temperatures, a process known as cold stamping. This deformation induces strain hardening, where the strain accumulates within the workpiece. Consequently, there is a need for increased forming force, a relationship often described by the Swift hardening [19] in Eq. (3).

$$\sigma = k(\varepsilon_0 + \varepsilon^p)^n \quad (3)$$

where *K* is strengthening coefficient and *n* is strain hardening exponent.

The value of n characterizes the true strain behaviour. A higher *n* value signifies a greater force necessity for subsequent forming procedures.

2.3. Drawing ratio

Flowability imposes a constraint on drawability, indicating the maximum attainable drawing ratio [20]. This value is determined by the material's drawing force, the initial diameter of the workpiece sheet, and the diameter of the punch. The drawability limit can be calculated using the formula by Eq. (4).

$$\beta_{max} = d_0/d_1 \tag{4}$$

where β_{max} is the maximum draw ratio, which is the ratio of the initial diameter of the workpiece sheet to the final diameter of the drawn part, d_0 is the initial diameter of the workpiece sheet and d_1 is the final diameter of the drawn part.

2.4. Barlat yield criteria

The Barlat 1989 yield criterion is often chosen for JAC270F steel because of its effectiveness in modelling anisotropic metals, such as those in automotive applications, where precise forming is critical. This criterion provides a simplified yet accurate representation of plastic behavior under planar stress states, using fewer parameters than other models. It accounts for the anisotropic nature of metals like JAC270F, enabling reliable predictions of formability and yielding patterns, which are essential in simulations for metal forming processes [21].

Since this research focuses on the forming of sheet metal materials, which exhibit anisotropic behavior (where the material properties vary in different rolling directions), the Barlat 1989 yield criterion [22] was chosen due to its high accuracy in describing steel materials. This criterion enhances the accuracy of the simulation results. Barlat 3-parameter model is defined as Eq. (5):

$$f = a|k_1 + k_2|^M + b|k_1 + k_2|^M + c|2k_2|^M = 2\bar{\sigma}^M \tag{5}$$

where Parameter k_1 and k_2 can be calculated from Eq. (6) and Eq. (7). Eq. (5):

$$k_1 = \frac{\sigma_{xx}+h\sigma_{yy}}{2} \tag{6}$$

$$k_2 = \left[\left(\frac{\sigma_{xx}-h\sigma_{yy}}{2}\right) + p^2\sigma_{xy}^2\right]^{\frac{1}{2}} \tag{7}$$

where Parameter *a, c, h* and *p* are also calculated from Eqs. (8)to (11):

$$a = 2 - 2\sqrt{\frac{r_0}{1+r_0}\cdot\frac{r_{90}}{1+r_{90}}} \tag{8}$$

$$c = 2\sqrt{\frac{r_0}{1+r_0}\cdot\frac{r_{90}}{1+r_{90}}} \tag{9}$$

$$h = \sqrt{\frac{r_0}{1+r_0}\cdot\frac{1+r_{90}}{r_{90}}} \tag{10}$$

$$p = \frac{\bar{\sigma}}{\tau_s}\left(\frac{2}{2a+2^{M}c}\right)^{\frac{1}{M}} \quad (11)$$

where p is the yield strength (MPa), $\bar{\sigma}$ is effective stress (MPa), τ_s is shear stress (MPa) and M is crystal structure factor: M = 6 for materials with a Body Centered Cubic (BCC) crystal structure and M = 8 for materials with a Face Centered Cubic (FCC) crystal structure.

2.5. Keeler-Brazier original equation

In this research, the Keeler equation [23] was chosen as the damage criterion, as it is one of the most widely used Forming Limit Curves (FLCs) for steel sheet materials. This criterion provides a reliable indication of critical damage areas in forming simulations, identifying regions on the workpiece that are likely to experience failure after the forming process. Its use enhances the reliability of the simulation results. In 1977, Keeler proposed equations for creating the Forming Limit Curve (FLC), considering the values of the work hardening exponent (n) and sheet thickness (t) to determine the FLC0, which is the lowest point on the FLC. The equation of FLC0 as shown in Eq. (12).

$$FLC_0 = \ln\left[1 + \left(\frac{23.3+14.13t}{100}\right)\frac{n}{0.21}\right] \quad (12)$$

The left side of FLC as shown in Eq. (13).

$$\varepsilon_1 = FLC_0 - \varepsilon_2 \quad (13)$$

The right side of FLC as shown in Eq. (14).

$$\varepsilon_1 = (1 + FLC_0)(1 + \varepsilon_2)^{0.5} - 1 \quad (14)$$

3. Finite Element Simulation of Forming Process

Finite element simulation of forming in this research utilizes AutoForm software, a specialized tool for automotive part forming. It provides a 3D representation of the part, as depicted in Fig. 6, which serves as the basis for the forming simulation. The simulation process is outlined in the flow chart displayed in Fig. 7.

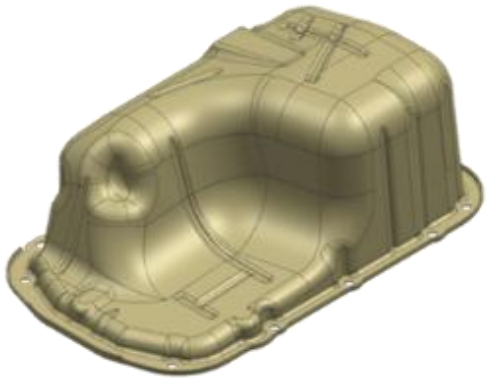

Fig. 6. 3D image of the part.

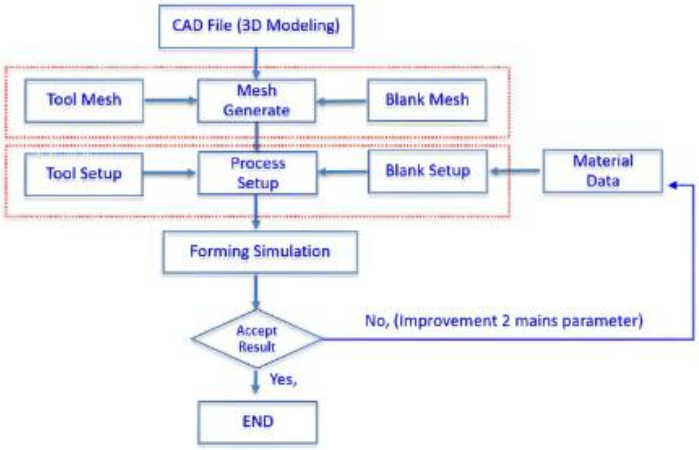

Fig. 7. Process flow chart of the simulation.

3.1. Tool and blank mesh generation

A mesh is generated for both the workpiece and the die set, which includes the punch, die, and blank holder. The software automatically generates the mesh for both the tool and the blank, assigning them as rigid elements. The element size for the workpiece is determined based on the requirements of the forming simulation, as illustrated in Fig. 8.

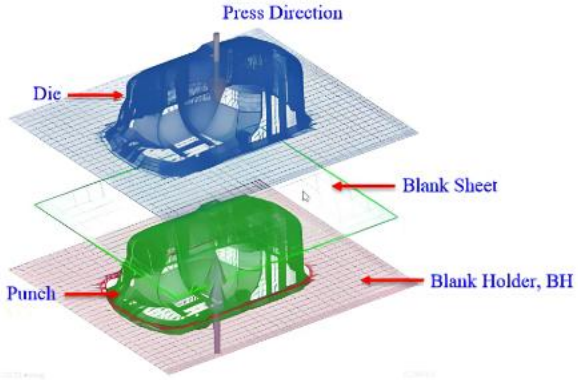

Fig. 8. Finite element model for simulation.

The AutoForm software automatically generates a mesh, dividing the domain into non-overlapping subdomains known as elements. Each element contains defined nodes. When combined, these elements form a mesh that can be analysed for this research. A three-node EPS-11 mesh starting at 10 millimetres is used, with elastic-plastic deformation in each element and 11 nodes corresponding to the workpiece thickness. Each node has five degrees of freedom, comprising two tangent vectors and a normal vector, along with rotation around the tangent axis. Mesh quality analysis is conducted at three levels, divided into four parts, following AutoForm software requirements.

3.2. Material properties input

The key parameters related to material properties, including those derived from the Barlat Yield Surface [21] and Swift hardening law, are essential inputs for the forming simulation. These parameters encompass the Young's modulus, the material's anisotropy across three rolling directions (0, 45, 90 degrees), and the choice of the Keeler Model for the forming limit curve (FLC) model [22]. These inputs are depicted in the parameter input window, as illustrated in Fig. 9.

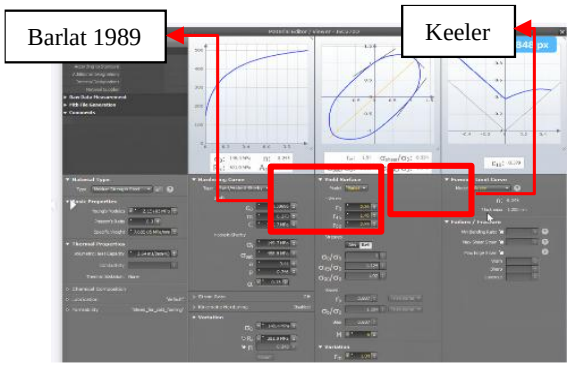

Fig. 9. Input of variable values in the forming model.

4. Simulation and Experimental Results

The simulation results from the AutoForm software display various types of defects occurring during the forming process, represented by different colour bands: the Purple area indicates increased thickness of the workpiece, the Blue area shows metal compression, the Gray area signifies no metal elongation, the Yellow area highlights a risk of tearing, the Orange area indicates increased thinning, and the Red area represents severe tearing of the workpiece.

4.1. Simulation results of single-process deep drawing

Single-process deep drawing validation was conducted, as illustrated in Fig. 10. This approach is desirable for die manufacturers aiming to minimize die manufacturing costs. Historically, dies for deep drawing of workpieces with similar shapes have been manufactured using two processes (deep drawing 1 and 2).

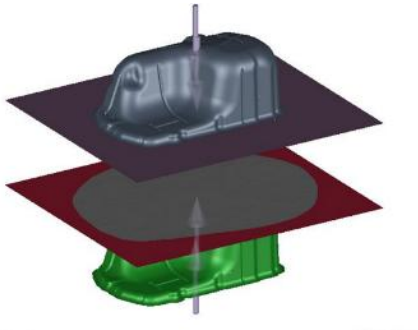

Fig. 10. Single-process deep drawing.

The effects of blank size

Validation of the simulation results for the deep draw forming process 1 (OP10 Draw-1) was conducted. The initial rough blank, with dimensions of width x length (371.30 x 447.60 mm), was obtained by unfolding the sheet size of the workpiece using simulation software, as depicted in Fig. 11(a). Analysis of the simulation results of the forming process revealed insufficient formability, as indicated in Fig. 11(b). It was observed that the size of the blank was unable to be formed adequately, particularly evident in the short edges around the workpiece. Additionally, severe wrinkling was observed during the forming process.

A preliminary blank scaling simulation was conducted to assess the feasibility of completing the first deep drawing process (OP10 Draw-1) in a single operation. The initial blank size was set to 371.30 mm x 447.60 mm. However, the simulation revealed insufficient flange size for subsequent forming processes, particularly along the short edges of the part, as depicted in Fig. 11(b). This inadequacy stemmed from metal flow issues following deep drawing. Furthermore, Fig. 11(c) illustrates severe wrinkling during forming, particularly in the curved slope area (highlighted in red). Metal compression in this region complicates metal flow, leading to accumulation and exacerbating wrinkling issues.

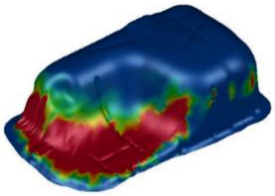

(a) Initial blank.

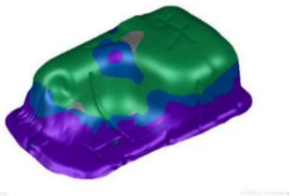

(b) Formability.

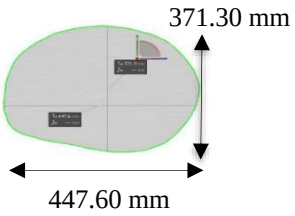

(c) Wrinkles.

Fig. 11. Simulation results of oil pan by initial blank size.

The rough blank was subsequently expanded by 20 mm (expansion of rough blank) to achieve a width x length of 410.30 x 483.80 mm, as illustrated in Fig. 12(a) with reference to the Reference Point. Forming simulation results, depicted in Fig. 12(b), indicate sufficient formability for the next forming process.

However, the persistent issue of severe wrinkling, as depicted in Fig. 12(c), remains unchanged. This wrinkling occurs due to metal compression in the overlapping curved corners, highlighted in red in Fig. 12(d). Despite the expansion of the rough blank size by 20 mm, the simulation shows no

improvement in eliminating severe wrinkling. Thus, completing the process in a single operation is not feasible.

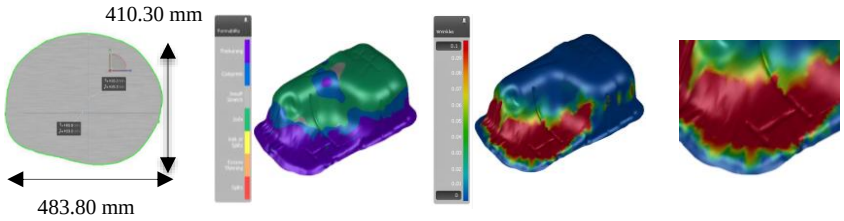

(a) Expanded blank size **(b) Formability** **(c) Wrinkles** **(d) Overlapping curved corners**

Fig. 12. Simulation results of oil pan by expanded blank size.

4.2. Simulation results of two-steps deep drawing process

Due to the issues encountered in the automotive manufacturing industry in Thailand, where the Oil Pan component could not be formed using a Single-Process Deep Drawing, a solution was proposed by using the Two-Steps Deep Drawing Process. However, the resulting part was still not sufficiently accurate. Therefore, the forming process of the Oil Pan component was simulated using the AutoForm program, with the aim of determining the most optimal values for blank holder force, die radius, and friction coefficient to successfully form the automotive part to completion.

4.2.1. Deep drawing process-01

From the issues highlighted in Fig. 12(d), it is evident that the problem of overlapping curved corners, as depicted in Fig. 13, cannot be addressed in a single desired process. Hence, it necessitates a secondary drawing in the subsequent process. To address this, the deep drawing process was bifurcated between the first and second drawing operations. The separation of the overlapping curved corners in the initial process aims to mitigate stress and metal flow, as illustrated in Fig. 14. Subsequently, the 3D CAD file depicted in Fig. 14(b) was utilized to simulate the drawing process and verify whether the desired outcomes for the first deep drawing process (OP10 Draw-01) could be achieved.

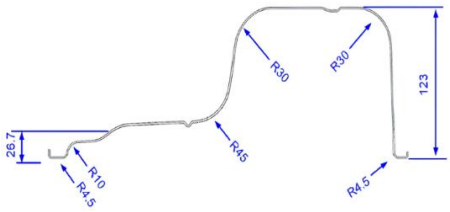

Fig. 13. Cross-sectional view of a workpiece with overlapping curved corners.

(a) Overlapping Curved Corners. (Before Improvement) **(b) Separated Curved Corners. (After Improvement)**

Fig. 14. Separation of overlapping curved corners.

The simulation results revealed slight wrinkling (indicated by green, yellow, and red areas) in certain regions of the workpiece along the curved radius, as depicted in Fig. 15. It is imperative to address this issue to prevent additional wrinkling. This simulation was undertaken to validate the outcomes of the deep drawing simulation and to ascertain the feasibility of successfully forming the OP10 Draw-01 process.

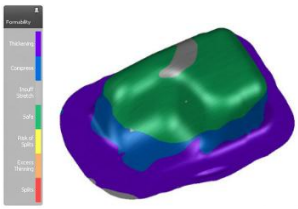

Fig. 15. Formability of deep drawing process-01.

4.2.2. Deep drawing process-02

After concluding the results from the simulation of deep drawing process 1 (OP10 Draw-1), the simulation of continuous deep drawing process 2 was conducted. The 3D workpiece file obtained from the simulation of process 1 was utilized. The simulation of deep drawing in process 2 encompassed areas with overlapping curved angles of the workpiece that could not be successfully drawn in process 1. The workpiece was drawn to a depth of 100 mm from the first draw, increased by another 25 mm, and the length of the workpiece in this process was extended by 32 mm from the initial 302 mm. The simulation results, depicted in Figs. 16(a) and (b), reveal severe tearing (splits) on the walls of the overlapping curved angles of the forming (indicated in green, yellow, and red), necessitating further improvements.

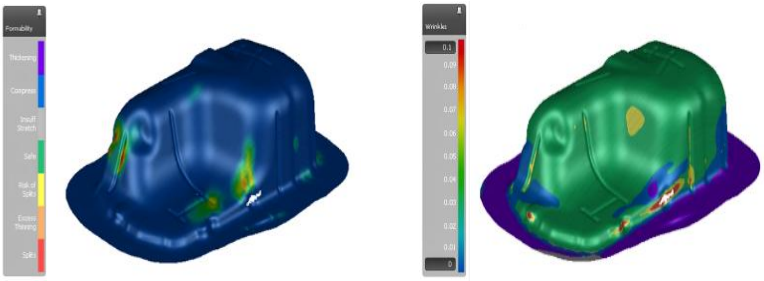

(a) Formability. **(b) Wrinkles.**

Fig. 16. Simulation results of workpiece from deep drawing process-02.

4.2.2.1. Effects of blank holder force in deep drawing process-02

For the effects of blank holder force (BHF), initially, the industry standard used a BHF of 10.50 tons. However, after forming, severe tearing was observed in the oil pan part, indicating that the BHF used was excessively high. Consequently, the researcher gradually reduced the BHF and simulated the oil pan forming process with varying BHF values. It was found that when the BHF was set to 7.50 tons, the automotive part achieved the best quality after forming. If the BHF is too low, significant wrinkling occurs in the workpiece.

Consequently, the blank holder force was reduced to 7.50 tons to alleviate the tensile stress from the original simulation. After rerunning the forming simulation, the results are displayed in Figs. 17(a) and (b). Severe tearing (splits) no longer occurs, but the workpiece still exhibits severe wrinkles on the workpiece wall at the same location as before but it to smaller.

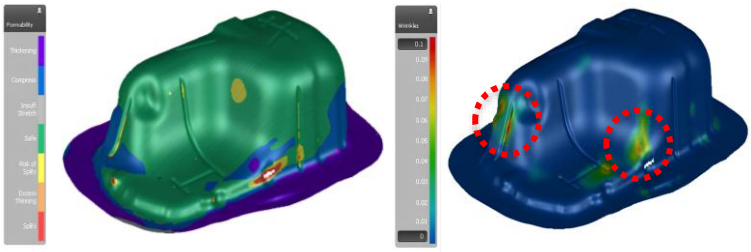

(a) Formability. **(b) Wrinkles.**

Fig. 17. Simulation results of workpiece by BHF of 10.50 tons.

4.2.2.2. Effects of die radius in deep drawing process-02

Initially, an issue was identified in the industry regarding the production of Oil Pan components, which had been designed with a die radius of 4.50 millimetres. However, forming could not be completed successfully due to tearing that occurred after the production process. Upon reviewing deep drawing theory, it was found that the die radius should be approximately 4 to 8 times the thickness of the metal used for deep drawing. Consequently, the die radius was adjusted to 6 times the workpiece thickness, resulting in a die radius of 7.20 mm, and further adjusted to 8 times the workpiece thickness, resulting in a die radius of 9.60 mm. The position of the “Die Radius”, as shown in the Fig. 18.

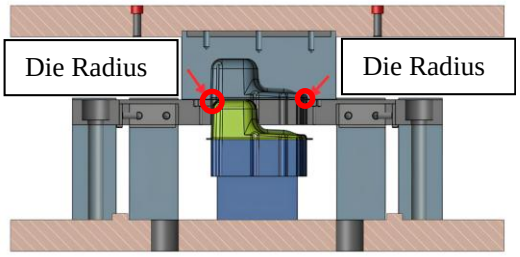

Fig. 18. The position of die radius.

After adjusting the initial die radius to 7.20 mm, the simulation results are depicted in Figs. 19(a) and (b). Wrinkles still occur in the forming process on the wall of the curved area at two points (highlighted in green, yellow, and red). The Figures 20(a) and b) show the simulation results of die radius 9.60 mm. Although wrinkles still occur on the wall of the curved area at two points (highlighted in green, yellow, and red), the size of the wrinkles is noticeably reduced compared to using a die radius of 7.20 mm. However, new wrinkles emerge in a different area along the reinforcement line at Straight Reinforcement, indicating the need for further adjustments to related factors.

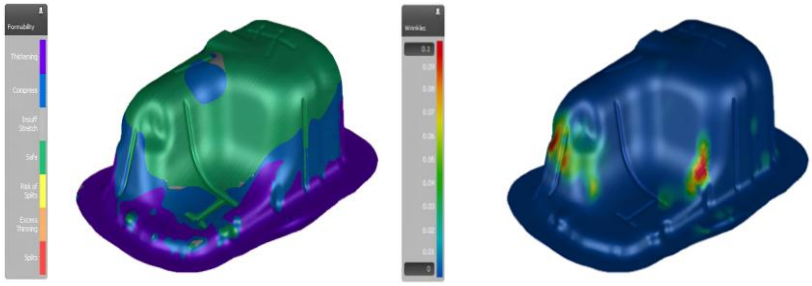

(a) Formability. **(b) Wrinkles.**

Fig. 19. Simulation results of workpiece by die radius of 7.2 mm.

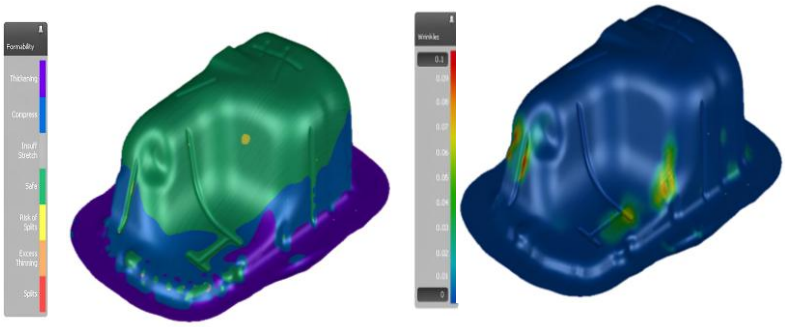

(a) Formability. **(b) Wrinkles.**

Fig. 20. Simulation results of workpiece by die radius of 9.6 mm.

4.2.2.3. Effects of friction coefficient

Initially, an issue was identified in the industry where forming the Oil Pan component was unsuccessful due to tearing, partly attributed to the friction coefficient. In the industry, castor oil is used as a lubricant, which results in a friction coefficient of 0.15 [24]. The researcher sought a new lubricant to reduce the friction coefficient in the Oil Pan forming process, identifying lard, which provides a friction coefficient of 0.11 [24]. By using lard as the new lubricant, the friction coefficient was reduced to 0.11. The simulation results in the AutoForm software, shown in Figs. 21(a) and (b), reveal that wrinkling still appears near the straight reinforcement line. However, the wrinkles on the walls of the workpiece show a decreasing trend compared to the previous results.

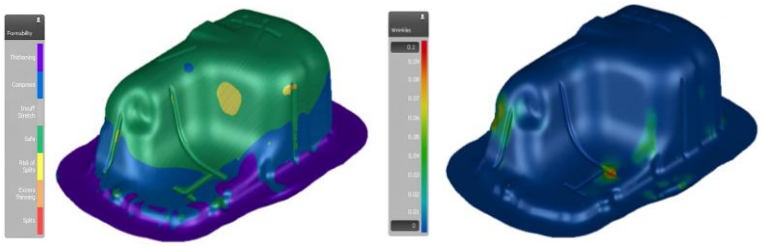

(a) Formability. **(b) Wrinkles.**

Fig. 21. Simulation results of workpiece by friction coefficient of 0.10.

4.3. Thinning results

After attaining the final acceptable simulation results, it is essential to assess the thinning of the workpiece following the forming simulation. The acceptable thinning value must not exceed 20 percent of the initial sheet metal thickness (rough blank), which is 1.20 mm. This criterion should be met at each section of the workpiece (Section) at three positions (Section A, B, and C) as depicted in Fig. 22. Upon evaluating the simulation results for thinning, it is confirmed that they fall within the 20 percent threshold. With the workpiece thickness (rough blank) maintained at 1.20 mm, the thinning does not exceed 20 percent of the initial sheet metal thickness. Therefore, the maximum acceptable thinning is determined to be 0.24 mm. The analysis indicates that no point on the workpiece exceeds the -0.24 mm thinning limit. Consequently, based on this criterion, the deep drawing process can be deemed acceptable.

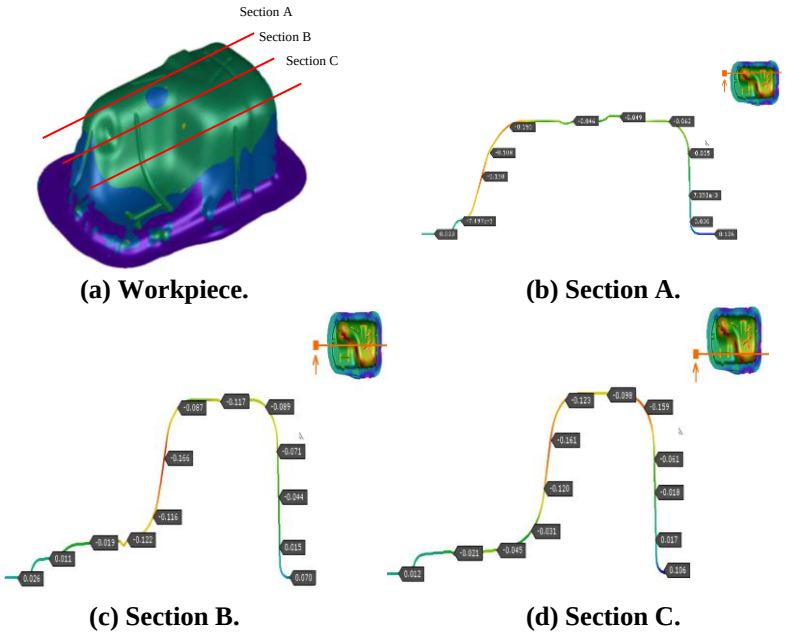

(a) Workpiece. **(b) Section A.**

(c) Section B. **(d) Section C.**

Fig. 22. Thickness of the workpiece after forming.

4.4. Springback results

Following the forming simulation, it is crucial to verify the thickness of the workpiece against the acceptable springback value of ±1.0 mm. Additionally, it's essential to consider the tolerance value and functional requirements of the workpiece at various locations on the vehicle, as specified by the automaker. Springback is inspected in three sections of the workpiece: Section A, Section B, and Section C, as shown in Fig. 23. The simulation results indicate that the thickness falls within the acceptable range of ±1.0 mm, ranging from -0.004 mm to 0.342 mm.

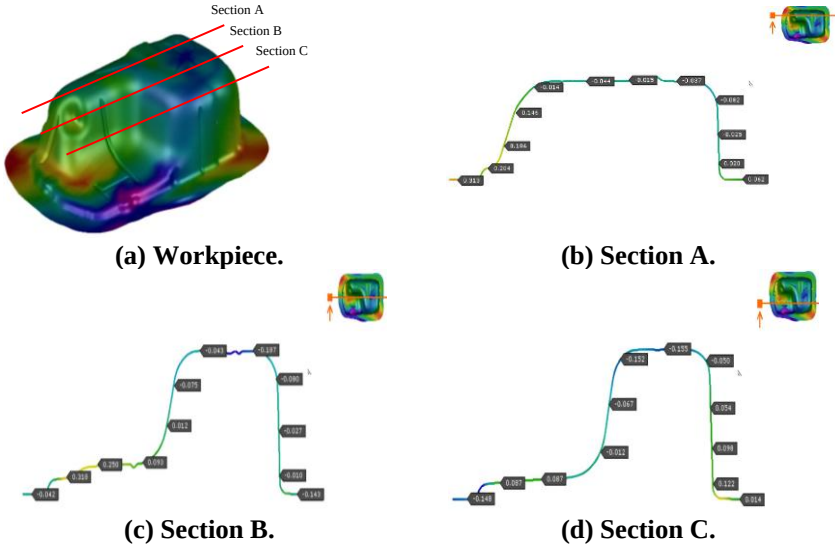

(a) Workpiece. **(b) Section A.**

(c) Section B. **(d) Section C.**

Fig. 23. Springback of the workpiece after forming.

4.5. Experimental results

4.5.1. Two-step deep drawing process results

From the study of parameters affecting the formability of sheet metal materials through the simulation of the Oil Pan component using the AutoForm program, the researcher selected a blank holder force (BHF) of 7.50 tons, a die radius of 9.6 mm, and a friction coefficient of 0.11. These conditions were found to be the optimal combination that prevented damage to the workpiece after the two-step forming process and were subsequently applied in real-world industrial production, as will be shown in the following section.

4.5.1.1. Deep drawing process-01

After obtaining the results from the forming simulation, the 3D workpiece file (CAD File) is utilized to design the die tooling. This comprises a deep draw die (Drawing Process-01), with the main structure of the die set made of FC300 grade cast iron (UPR and LWR Die). The internal structure of the punch and die sets can be replaced with punch and die inserts. Tool steel (Grade DCMX) is employed after heat treatment and then coated to reduce friction during forming (TD Coating). The deep drawing process will utilize a 600-ton hydraulic press machine with a cushion

post of the machine serving as the blank holder, as depicted in Fig. 24. Also, Fig. 25 clearly presents the actual part after deep drawing process-01.

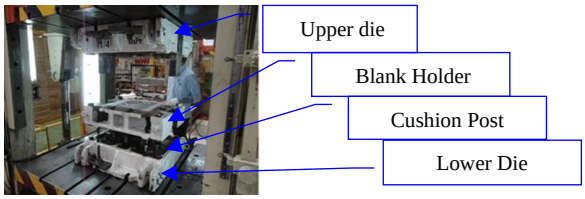

Fig. 24. Die set for deep drawing process-01.

Fig. 25. The actual part after deep drawing process-01.

4.5.1.2. Deep drawing process-02

After obtaining the results from the forming simulation, the 3D workpiece file (CAD File) was utilized to design the die tooling. This pertains to the second deep drawing die (Drawing Process-02). The main structure of the die set is crafted from FC300 grade cast iron (UPR and LWR Die), with the internal structure of the punch and die sets designed for potential replacement when significantly damaged (Punch and Die Insert). Tool steel (Grade DCMX), post-heat treatment, is coated to mitigate friction during forming (TD Coating). The deep drawing process will employ a 600-ton hydraulic press machine, with the cushion post of the machine serving as the blank holder, as illustrated in Fig. 26. Also, Fig. 27 clearly presents the actual part after deep drawing process-02.

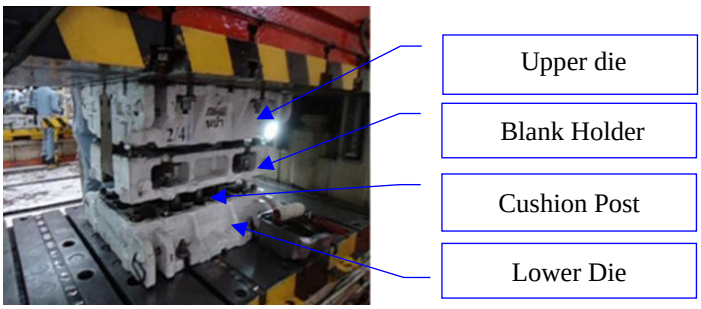

Fig. 26. Die set for deep drawing process-02.

Fig. 27. Actual part after deep drawing process-02.

4.6. Comparison of thinning and springback on the B-section between simulation and experimental results

Tables 2 and demonstrate the comparison of sheet thinning and springback results on the B-section between forming simulation and experiment, respectively.

Table 2. Comparison of sheet thinning results between forming simulation and experiment.

Thinning point	Methodology	
	FEM (mm)	Experimental (mm)
1	0.104	0.123
2	-0.017	-0.010
3	-0.061	-0.056
4	-0.081	-0.079
5	-0.097	-0.090
6	-0.104	-0.110
7	-0.011	-0.008
8	0.027	0.019
Min (mm)	-0.104	-0.110
%Differences	5.45%	

Table 3. Comparison of springback results between forming simulation and experiment.

Springback point	Methodology	
	FEM (mm)	Experimental (mm)
1	0.182	0.170
2	0.067	0.059
3	-0.152	-0.149
4	-0.013	-0.018
5	0.028	0.030
6	0.080	0.079
7	0.309	0.300
8	0.027	-0.010
9	-0.004	-0.067
Min (mm)	-0.152	-0.149
%Differences	2.01%	

5. Conclusions

This research presents a solution for forming the Oil Pan component, made from JAC270F sheet metal with a thickness of 1.2 mm, using a new process called the Two-Steps Deep Drawing Process. The forming of the Oil Pan was simulated using the AutoForm program, incorporating material models such as the Barlat 1989 yield function, Swift hardening law, and the forming limit curve based on the Keeler equation to ensure the highest accuracy in the simulation. Additionally, finite element method (FEM) simulations by AutoForm were used to determine the optimal parameters for the Oil Pan forming process, including blank holder force, die radius, and friction coefficient. The conclusions of this research are as follows:

- This research presents a new forming method for the Oil Pan component, called the Two-Steps Deep Drawing Process, as an alternative to the Single-Steps Deep Drawing Process. The results demonstrate that the two-step process allows successful forming of automotive parts. This success is due to the Oil Pan component's considerable height, which makes it impossible to form in a single step. Therefore, the forming process was divided into two stages, enabling the sheet to be successfully shaped into the Oil Pan.
- The Blank Holder Force (BHF) is another critical factor that significantly affects the formability of sheet metal materials. If the BHF is set too high during the forming process, it can make it difficult for the material to flow. This lack of material flow leads to tearing during the forming process. On the other hand, if the BHF is set too low, the material will flow too easily, resulting in wrinkling on the workpiece. Therefore, it is essential to select the appropriate BHF for each material. In this research, it was concluded that for forming the Oil Pan component, a BHF of 7.50 tons should be used, compared to the original value of 10.50 tons, which was too high.
- Regarding the Die radius, initially, an issue was identified in the industry where the Oil Pan component was designed with a die radius of 4.50 millimetres. However, the forming process was unsuccessful due to tearing that occurred after production. The researcher found that according to theory, the die radius should be approximately 4 to 8 times the thickness of the metal being formed. As a result, the die radius was adjusted to 6 times the workpiece thickness, resulting in a value of 7.20 mm, and further adjusted to 8 times the workpiece thickness, resulting in a value of 9.60 mm. The simulation results in AutoForm showed that a die radius of 9.60 mm minimized wrinkling and damage to the Oil Pan component after the forming process. If the die radius is too low, it makes it difficult for the material to flow, leading to tearing during forming. Conversely, if the die radius is too high, the material flows too easily, which results in wrinkling on the workpiece. Therefore, it is crucial to select an appropriate die radius, ideally within the range of 4 to 8 times the thickness of the metal.
- The final variable in this research is the friction coefficient. Initially, in the industry, castor oil was used as the lubricant, resulting in a friction coefficient of 0.15. The researcher then sought a new lubricant to reduce the friction coefficient during the Oil Pan forming process, leading to the use of lard, which reduced the friction coefficient to 0.11. This adjustment allowed for successful forming of the Oil Pan component. In deep drawing processes, a high friction coefficient negatively impacts material flow, making it difficult for the material to deform properly.

- From the study of parameters affecting the formability of sheet metal materials through the simulation of the Oil Pan component using the AutoForm program, it was concluded that a blank holder force (BHF) of 7.50 tons, a die radius of 9.6 mm, and a friction coefficient of 0.11 should be used. These conditions were found to be the optimal combination that prevents damage to the workpiece after the two-step forming process. When the Oil Pan component was formed using these optimal conditions, the simulation results showed that the forming process was successfully completed without any damage.
- In this research, the accuracy of the simulation was checked by comparing the thinning and springback values from the AutoForm simulation with those from actual automotive part forming in the industry using the same forming conditions. The results showed that the AutoForm simulation of the Oil Pan component, using material models such as the Barlat 1989 yield function, Swift hardening law, and the forming limit curve by the Keeler equation, is highly reliable. The discrepancies between the FEA results and actual forming were only 5.45% for thinning and 2.01% for springback, respectively.

The "Multi-Step Deep Drawing Process" is a novel and highly intriguing technique, with limited application of existing knowledge in real automotive component manufacturing. This research acknowledges certain limitations, particularly in the availability of advanced testing equipment for material properties, leading to the selection of less complex material models.

Numerous variables potentially influencing this process still warrant further future study, including the design of each forming step and the distribution of part height at each step. Exploring these factors could enable the successful formation of complex automotive components and support the adaptation of this technique for forming higher-strength automotive materials, which are inherently more challenging to shape.

Nomenclatures

FLC_0	The lowest point on the Forming Limit Curves
K	Strengthening coefficient
M	Crystal structure factor
n	Strain hardening exponent
r	The r-value
$\bar{r}$	The average r-value
r_0	The r-values in the 0-degree directions
r_{45}	The r-values in the 45-degree directions
r_{90}	The r-values in the 90-degree directions

Greek Symbols

β_{max}	The maximum draw ratio
ε_1	Major strain
ε_2	Minor strain
ε_t	Thickness strain
ε_w	Width strain
$\bar{\sigma}$	Effective stress, MPa
τ_s	Shear stress, MPa

σ	Stress, MPa

Abbreviations

FLC	Forming Limit Curves

References

1. Özdilli, O. (2020). An investigation of the effects of a sheet material type and thickness selection on formability in the production of the engine oil pan with the deep drawing method. *International Journal of Automotive Science and Technology*, 4(4), 198–205.
2. Colgan, M.; and Monaghan, J. (2003). Deep drawing process: Analysis and experiment. *Journal of Materials Processing Technology*, 132(1-3), 35-41.
3. Hosseini, R.; EBRAHIMI, M.M.; and Asa, A. (2012). An investigation into the effects of friction and anisotropy coefficients and work hardening exponent on deep drawing with FEM. *Journal of Advanced Materials and Processing*, 1(2), 39-49.
4. Ikumapayi, O.M.; Afolalu, S.A.; Kayode, J.F.; Kazeem, R.A.; and Akande, S. (2022). A concise overview of deep drawing in the metal forming operation. *Materials Today: Proceedings*, 62, 3233-3238.
5. Akafzadeh, E.; Salmani-Tehrani, M.; and Shayan, M. (2022). Deep drawing of a thin hemispherical cup using a novel die without a blank holder: Experimental and numerical investigations. *Journal of the Brazilian Society of Mechanical Sciences and Engineering*, 44(7), 281-293.
6. Altan, T.; and Tekkaya, A.E. (2012). *Sheet Metal Forming: Fundamentals*. ASM International.
7. Altan, T.; and Tekkaya, A.E. (2012). *Sheet Metal Forming: Processes and Applications*. ASM International.
8. Buranathiti, T.; Cao, J.; Xia, Z.C.; and Chen, W. (2015). Probabilistic design in a sheet metal stamping process under failure analysis. *AIP Conference Proceedings*, 778(1), 867-872.
9. Ghafar, A.A.; Abdullah, A.B.; and Mahmood, J.I. (2021). Experimental and numerical prediction on square cup punch-die misalignment during the deep drawing process. *The International Journal of Advanced Manufacturing Technology*, 113, 379-388.
10. Nakagawa, K.; Yamasaki, Y.; Tamai, Y.; and Hiramoto, J. (2022). Influence of 1st step shape on formability of circular truncated cone stretch forming in two-step forming. *Materials Transactions*, 63(3), 311-318.
11. Suranuntchai, S. (2008). Finite element analysis of sheet metal under drawing processes for body brake booster. *Science and Technology Asia*, 13(4), 48-53.
12. Qin, T. (2020). Finite Element Analysis of the Deep-drawing Stress of QT8812 Automobile Engine Oil Pan. *Proceedings of the 2nd International Conference on Big Data and Artificial Intelligence* (*ISBDAI*), Johannesburg, South Africa, 583-588.
13. Yoshihara, S.; Manabe, K.I.; and Nishimura, H. (2005). Effect of blank holder force control in deep-drawing process of magnesium alloy sheet. *Journal of Materials Processing Technology*, 170(3), 579-585.

14. Booranacheep, C.; Thanadngarn, C.; and Buakaew, V. (2007). Analysis of wrinkle behaviors using forming limit diagrams. (in Thai). *Proceedings of the* 21*st Mechanical Engineering Network of Thailand*, Chonburi, 1004-1009.
15. Jurendić, S.; and Gaiani, S. (2011). Deep drawing simulation of α-titanium alloys using LS-Dyna. *Proceeding of the 8th European LS-DYNA Users Conference*, Strasbourg, 1-8.
16. Suwanchinda, B.; and Suranuntchai, S. (2016). Development of forming processes for high strength steel automotive parts by finite element simulation: Case study on BRACKET, FR BUMPER SIDE LH/RH. *KMUTT Research and Development Journal*, 39(4), 615-628.
17. Panich, S.; Uthaisangsuk, V.; Juntaratin, J., and Suranuntchai, S. (2011). Determination of Forming Limit Stress Diagram for Formability Prediction of SPCE 270 Steel Sheet. *Journal of Metals, Materials and Minerals*, 21(1), 19-27.
18. Hu, J.; Marciniak, Z.; and Duncan, J. (2002). *Mechanics of sheet metal forming*. Elsevier.
19. Swift, H. (1952). Plastic instability under plane stress. *Journal of the Mechanics and Physics of Solids*, 1(1), 1-18.
20. Valberg, H.S. (2010). *Applied metal forming: Including FEM analysis*. Cambridge University Press.
21. Chen, L.; Zhang, H.; and Song, M. (2020). Extension of Barlat's yield criterion to tension–compression asymmetry: Modeling and verification. *Metals*, 10(6), 1-20.
22. Barlat, F.; and Lian, K. (1989). Plastic behaviour and stretchability of sheet metals. Part I: A yield function for orthotropic sheets under plane stress conditions. *International Journal of Plasticity*, 5(1), 51-66.
23. Keeler, S.P. (1965). Determination of forming limits in automotive stampings. *SAE Technical Paper* 650535.
24. Engineering ToolBox. (2004). Friction - Friction coefficients and calculator. Retrieved November 9, 2024, from https://www.engineeringtoolbox.com/friction-coefficients-d_778.html